Monthly Notices
of the
ROYAL ASTRONOMICAL SOCIETY

MNRAS **495,** L22–L26 (2020)
Advance Access publication 2020 March 19

doi:10.1093/mnrasl/slaa047

Star formation law in the epoch of reionization from [C II] and C III] lines

L. Vallini [1]★ A. Ferrara,[2] A. Pallottini [2,3] S. Carniani [2] and S. Gallerani[2]

[1]*Leiden Observatory, Leiden University, PO Box 9500, NL-2300 RA Leiden, the Netherlands*
[2]*Scuola Normale Superiore, Piazza dei Cavalieri 7, I-56126 Pisa, Italy*
[3]*Centro Fermi, Museo Storico della Fisica e Centro Studi e Ricerche 'Enrico Fermi', Piazza del Viminale 1, Roma I-00184, Italy*

Accepted 2020 March 12. Received 2020 March 10; in original form 2020 February 3

ABSTRACT

We present a novel method to simultaneously characterize the star formation law and the interstellar medium properties of galaxies in the epoch of reionization (EoR) through the combination of [C II] 158 μm (and its known relation with star formation rate) and C III] λ1909 Å emission line data. The method, based on a Markov chain Monte Carlo algorithm, allows us to determine the target galaxy average density, n, gas metallicity, Z, and 'burstiness' parameter, κ_s, quantifying deviations from the Kennicutt–Schmidt relation. As an application, we consider COS-3018 ($z = 6.854$), the only EoR Lyman Break Galaxy so far detected in both [C II] and C III]. We show that COS-3018 is a moderate starburst ($\kappa_s \approx 3$), with $Z \approx 0.4\,Z_\odot$, and $n \approx 500\,\mathrm{cm}^{-3}$. Our method will be optimally applied to joint ALMA and *James Webb Space Telescope* targets.

Key words: photodissociation region (PDR) – galaxies: high-redshift – galaxies: ISM.

1 INTRODUCTION

How do galaxies convert their gas into stars? How do their interstellar medium (ISM) properties influence star formation? Answers to these questions hold the key to understand galaxy evolution (see Dayal & Ferrara 2018, for a review).

In nearby galaxies and at intermediate redshifts, the so-called Kennicutt–Schmidt (KS) law (Schmidt 1959; Kennicutt 1998; de los Reyes & Kennicutt 2019), relating the star formation rate (SFR) and the gas surface density, is well established. Dozens of observational studies ranging from the local Universe (e.g. Bigiel et al. 2008; Schruba et al. 2011) up to $z \approx 3$–4 (e.g. Daddi et al. 2010; Tacconi et al. 2013; Genzel et al. 2015; Hodge et al. 2015) have shown that, when averaged over kpc scales, the SFR, $\Sigma_{\rm SFR}$, and the cold gas, $\Sigma_{\rm gas}$, surface density in disc galaxies follow a tight relation,

$$\Sigma_{\rm SFR} = 10^{-12}\kappa_s \Sigma_{\rm g}^{m}, \qquad (m \approx 1.4) \qquad (1)$$

valid over about 5 dex in $\Sigma_{\rm gas}$ (Heiderman et al. 2010). Two different SF regimes can be identified in the $\Sigma_{\rm SFR}$–$\Sigma_{\rm gas}$ plane: 'quiescent' ($\kappa_s \approx 1$) and 'starburst' ($\kappa_s > 1$) galaxies (Daddi et al. 2010; Hodge et al. 2015). However, as we move towards the epoch of reionization (EoR; $z > 6$), a precise assessment of the KS relation becomes progressively more difficult or even impossible. Advanced optical/near-infrared facilities such as the *Hubble Space Telescope*, Very Large Telescope (VLT), Keck, and Subaru telescopes enabled rest-frame ultraviolet (UV) continuum and line emission detection in large samples of EoR galaxies (e.g. Bouwens et al. 2015). The exquisite spatial resolution of such instruments often allows us to carry out UV size measurements (e.g. Shibuya, Ouchi & Harikane 2015; Curtis-Lake et al. 2016; Bowler et al. 2017; Kawamata et al. 2018; Matthee et al. 2019), hence enabling estimates of $\Sigma_{\rm SFR}$ in EoR galaxies.

Spatially resolved detections of cold gas tracers such as the CO lines in these systems are instead still very challenging or lacking (e.g. D'Odorico et al. 2018; Vallini et al. 2018; Pavesi et al. 2019). Low-J ($J \leq 3$) CO rotational transition detections in quiescent star-forming galaxies are still limited to $z \lesssim 3$ (Tacconi et al. 2013; Genzel et al. 2015) while at $3 < z < 4.5$ only few significant detections have been reported, either in massive submillimetre galaxies (Hodge et al. 2015; Sharda et al. 2018, 2019) or strongly lensed systems (Coppin et al. 2007; Dessauges-Zavadsky et al. 2015). Besides CO, alternative tracers such as the [C II] 158 μm emission, calibrated at $z \approx 1$, have been proposed to measure the gas mass (Zanella et al. 2018). However, Pavesi et al. (2019) pointed out that a full characterization of the ISM in EoR galaxies requires, in addition to [C II], information on CO or an ionized gas tracer.

In the last years, Atacama Large Millimeter Array (ALMA; Carilli & Walter 2013) has opened a new window on the ISM properties of early galaxies, allowing for the first time the detection at high spatial resolution and sensitivities of the 158 μm $^2P_{3/2} \rightarrow {}^2P_{1/2}$ transition of ionized carbon ([C II]) (e.g. Capak et al. 2015; Maiolino et al. 2015; Carniani et al. 2018; Smit et al. 2018; Hashimoto et al. 2019; Matthee et al. 2019). [C II] is the most luminous line in the far-infrared (FIR) band (Hollenbach & Tielens 1999), and traces cold neutral/molecular gas associated with photodissociation regions (PDRs; e.g. Vallini et al. 2015; Pallottini et al. 2017; Ferrara et al. 2019).

★ E-mail: vallini@strw.leidenuniv.nl

Importantly, the *James Webb Space Telescope* (*JWST*) will soon provide a complementary probe of the high-z ISM, targeting rest-frame optical/UV emission lines associated with ionized gas. Among the various UV line tracers, current state-of-the-art observational campaigns with, e.g. VLT and KECK (e.g. Stark et al. 2015, 2017; Ding et al. 2017; Laporte et al. 2017; Mainali et al. 2018; Hutchison et al. 2019) and theoretical studies (Feltre, Charlot & Gutkin 2016; Jaskot & Ravindranath 2016; Nakajima et al. 2018) showed that low-metallicity, $z > 5$ galaxies are expected to show prominent C III] λ1909 Å line emission. Such a line will be likely detected in large samples of galaxies with *JWST*, opening an interesting synergy with ALMA in targeting carbon lines. In this work we show that, by combining [C II] 158 μm and C III] λ1909 Å data, it is possible to constrain *at the same time* the KS relation and ISM properties of EoR galaxies. After presenting the method in Section 2, in Section 3 we apply it to COS-3018555981 at $z = 6.854$, the only Lyman Break Galaxy (LBG) representative of quiescent star-forming galaxies so far detected at $z > 6.5$ in [C II] and C III]. In Section 4 we discuss the implications of the results and our conclusions.

2 METHOD

Our method is based on an extension of the physical model for the [C II] emission in galaxies presented in Ferrara et al. (2019, F19 hereafter). While locally a tight $\Sigma_{\rm [C\,II]}$–$\Sigma_{\rm SFR}$ correlation has been measured (De Looze et al. 2014; Herrera-Camus et al. 2015), many EoR galaxies show $\Sigma_{\rm [C\,II]}$ values almost systematically fainter than expected from their measured $\Sigma_{\rm SFR}$ (Carniani et al. 2018; Pallottini et al. 2019).

F19 argued that three factors can produce such a deficit: (a) a high 'burstiness' parameter $\kappa_{\rm s}$ (see equation 1); (b) a low gas density n; (c) a low gas metallicity Z, with (b) and (c) playing a subdominant role. If a third observed quantity, besides $\Sigma_{\rm [C\,II]}$ and the deviation, $\Delta_{\rm [C\,II]}$, from the local $\Sigma_{\rm [C\,II]}$–$\Sigma_{\rm SFR}$ relation is available, then the n, Z, and $\kappa_{\rm s}$ degeneracy can be broken, thus enabling a complete characterization of the ISM properties and star formation law in EoR galaxies.

C III] is an excellent additional candidate line to break the degeneracy. In fact, contrary to the [C II] line, its luminosity at fixed $\Sigma_{\rm SFR}$ grows with $\kappa_{\rm s}$ due to the progressively thicker ionized layer (F19). Moreover, the $\Sigma_{\rm C\,III]}/\Sigma_{\rm [C\,II]}$ ratio is unaffected by the (unknown) relative abundances of different elements at high-z. In what follows we summarize the basic equations of our model, and operationally define $\Delta_{\rm [C\,II]}$. We refer the interested reader to F19 for a complete derivation of the equations.

2.1 [C II] emission model

Consider a disc galaxy with mean gas density n, carbon abundance $\mathcal{A}_{\rm C} = 2.7 \times 10^{-4}$ (Asplund et al. 2009), metallicity Z, and ionization parameter $U = n_\gamma/n$. The [C II] surface brightness [$\rm L_\odot\,kpc^{-2}$] can be written (F19, equation 35) as

$$\Sigma_{\rm [C\,II]} = 2.4 \times 10^9\, F_{\rm [C\,II]}(n, Z, U), \tag{2}$$

where $F_{\rm [C\,II]} = f^i_{\rm [C\,II]} + f^n_{\rm [C\,II]}$ (in $\rm erg\,s^{-1}\,cm^{-2}$) is the emerging [C II] flux. The first term in the previous equation accounts for the emission due to collision of C^+ ions with e^- in the ionized layer:

$$f^i_{\rm [C\,II]} = n_{\rm e}\Lambda^{(4)}_{\rm e} Z \mathcal{A}_{\rm C} N_{\rm H\,I}(Z, U), \tag{3}$$

where $n_{\rm e} \approx n$ is the number density of free electrons, $\Lambda^{(4)}_{\rm e}(T = 10^4\,{\rm K}) = 1.2 \times 10^{-21}$ erg $\rm cm^3\,s^{-1}$ is the cooling rate (Appendix B, F19), and $N_{\rm C\,II} \approx \mathcal{A}_{\rm C} Z N_{\rm H\,I}$ is the C^+ column density in the ionized layer. The second term, $f^n_{\rm [C\,II]}$, accounts for the emission due to collisions with H atoms in the neutral ($T = 10^2$ K) part of the PDR:

$$f^n_{\rm [C\,II]} = n\Lambda^{(2)}_{\rm H} \mathcal{A}_{\rm C} Z N_{\rm PDR}(Z, U). \tag{4}$$

In the previous equation, n is the H I number density; $\Lambda^{(2)}_{\rm H} = 7.65 \times 10^{-24}$ erg $\rm cm^3\,s^{-1}$ is the collisional cooling rate (Appendix B, F19), and the C II column density is $N_{\rm C\,II} \approx \mathcal{A}_{\rm C} Z N_{\rm PDR}$. In equations (3) and (4), $N_{\rm H\,I}$ and $N_{\rm PDR}$ depend on the dust shielding of the intensity (parametrized by U) of the ionizing interstellar radiation field. We assume a constant dust-to-gas ratio, so that the dust column density providing the extinction is $\propto Z$. We rewrite equation (15) of F19 in terms of these two quantities:

$$N_{\rm H\,I} = 3.7 \times 10^{17} \ln\left(1 - \frac{1 + 59Z\,U}{1 + 21.7Z\,U}\right); \tag{5}$$

we also use equation (30) of F19 to write

$$N_{\rm PDR} = \min\left[\frac{1.7 \times 10^{21}}{Z} \ln\left(1 + \frac{10^5 U}{1 + 0.9Z^{1/2}}\right),\, N_0\right] - N_i, \tag{6}$$

where N_0 is the disc total gas column density, and

$$N_i = 1.7 \times 10^{21} Z^{-1} \ln\frac{1 + 59ZU}{1 + 21.7ZU} \tag{7}$$

is the ionized layer column density (equation 14, F19).

Finally, U can be related to the gas surface density, $\Sigma_{\rm gas} = 7.5 \times 10^7 N_{0,22}\,\rm M_\odot\,kpc^{-2}$ (F19), and to $\Sigma_{\rm SFR}$ as

$$U = 1.7 \times 10^{14} \frac{\Sigma_{\rm SFR}}{\Sigma_{\rm g}^2} \simeq 10^{-3}\,\kappa_{\rm s}^{10/7}\,\Sigma_{\rm SFR}^{-3/7}, \tag{8}$$

where we substituted the KS relation (equation 1) to extract the dependence on κ_s. From equation (2), we then predict[1] the $\Sigma_{\rm [C\,II]}$–$\Sigma_{\rm SFR}$ relation for a given set (n, Z, $\kappa_{\rm s}$):

$$\Sigma_{\rm [C\,II]} = 2.4 \times 10^9\, F_{\rm [C\,II]}(\Sigma_{\rm SFR}|n, Z, \kappa_{\rm s}). \tag{9}$$

2.2 C III] emission model

Following the same reasoning outlined in Section 2.1, the C III] surface brightness can be written as

$$\Sigma_{\rm C\,III]} = 2.4 \times 10^9\, F_{\rm C\,III]}(n, Z, U). \tag{10}$$

The C III] emission is produced by the collisional excitation of C^{2+} ions by free electrons. Hence,

$$F_{\rm C\,III]} = n_{\rm e}\Lambda_{\rm C\,III]} \mathcal{A}_{\rm C} Z N_i(Z, U), \tag{11}$$

where the cooling rate at $T = 10^4$ K is $\Lambda^{(4)}_{\rm C\,III]} = 5.8 \times 10^{-22}$ erg $\rm cm^3\,s^{-1}$ (Appendix B, F19), and the C^{2+} column density is $N_{\rm C\,III} \simeq \mathcal{A}_{\rm C} Z N_i$, with N_i as in equation (7). We use equation (10) to predict the $\Sigma_{\rm C\,III]}$–$\Sigma_{\rm SFR}$ relation for a given set (n, Z, $\kappa_{\rm s}$):

$$\Sigma_{\rm C\,III]} = 2.4 \times 10^9\, F_{\rm C\,III]}(\Sigma_{\rm SFR}|n, Z, \kappa_{\rm s}). \tag{12}$$

2.3 Deviations from the local $\Sigma_{\rm [C\,II]}$–Σ_* relation

In the local Universe, a well-assessed $\Sigma_{\rm [C\,II]}$–$\Sigma_{\rm SFR}$ relation is found in spiral (Herrera-Camus et al. 2015) and low-metallicity dwarf

[1]The [C II] flux obtained with the above analytical model has been shown to be in excellent agreement with CLOUDY (Ferland et al. 2017) full RT calculations (fig. 3, F19).

galaxies (De Looze et al. 2014). In the last few years, the extension of such a relation to EoR galaxies has become feasible thanks to the high spatial resolution of ALMA observations. As noted by, e.g. Carniani et al. (2018) and F19, most of the sources at $z > 5$ are found to have $\Sigma_{[\rm C\,II]}$ values fainter than expected on the basis of the local relation. In what follows, we will adopt the following functional form of the $\Sigma_{[\rm C\,II]}$–$\Sigma_{\rm SFR}$ relation:

$$0.93 \log \Sigma^{\rm local}_{[\rm C\,II]} = \log \Sigma_{\rm SFR} + 6.99, \quad (13)$$

which has a small 1σ dispersion of 0.32 dex. This is obtained by De Looze et al. (2014) for low-metallicity dwarf galaxies. We checked that using a different relation (e.g. Herrera-Camus et al. 2015) does not affect our results. These systems are usually considered to be fair analogues of reionization sources. We define the expected deviation from the local $\Sigma_{[\rm C\,II]}$ relation (at fixed $\Sigma_{\rm SFR}$) as

$$\Delta_{[\rm C\,II]}(\Sigma_{\rm SFR}|n, Z, \kappa_{\rm s}) \equiv \log\ \Sigma_{[\rm C\,II]} - \log\ \Sigma^{\rm local}_{[\rm C\,II]}. \quad (14)$$

Note that is $\Delta_{[\rm C\,II]}$ is a function of the three parameters ($\kappa_{\rm s}$, n, and Z). As a caveat, it is worth stressing that: (i) in some cases the complex morphology of early galaxies (e.g. Kohandel et al. 2019) makes the determination of the actual size of the [C II]-emitting region somewhat challenging; (ii) in the local $\Sigma_{[\rm C\,II]}$–$\Sigma_{\rm SFR}$ calibration, the SFR is obtained both by optical lines (e.g. Hα) and the FIR continuum. On the contrary, the $\Sigma_{\rm SFR}$ in EoR galaxies is often derived from the UV continuum only, as the majority of high-z sources are undetected in dust continuum, and those detected have only one point on the dust continuum Spectral Energy Distribution (SED). This makes the determination of the total infrared luminosity highly dependent on the unknown dust temperature (Behrens et al. 2018).

2.4 Parameters derivation

Equations (9), (12), and (14) allow us to solve for the three unknown parameters ($\kappa_{\rm s}$, n, and Z). Our solution method is based on a Bayesian Markov chain Monte Carlo (MCMC) framework. We use the χ^2 likelihood function to fit the observed $\Sigma_{[\rm C\,II]}$, $\Sigma_{\rm C\,III]}$, and $\Delta_{[\rm C\,II]}$ of a galaxy and determine the posterior probability distribution of the model parameters. This choice enables us to fully characterize any potential degeneracies between our model parameters, while also providing the individual probability distribution functions (PDFs) for each of them. In this work we use the open-source `emcee` Python implementation (Foreman-Mackey et al. 2013) of the Goodman and Weare's Affine Invariant MCMC Ensemble sampler (Goodman & Weare 2010).

3 A CASE STUDY: COS-3018

As a case study, we apply our model to COS-3018555981 (COS-3018 hereafter), the only LBG (Smit et al. 2018) in the EoR ($z \approx 6.85$) so far detected both in [C II] and C III] (Laporte et al. 2017; Smit et al. 2018)[2]

COS-3018 was first discovered by Tilvi et al. (2013) and Bowler et al. (2014), and then re-analysed by Smit et al. (2015) as a part of their selection of IRAC excess sources in the 3.6 or 4.5 μm photometric bands deriving $z_{\rm phot} = 6.76$. Smit et al. (2018) spectroscopically confirmed the source at $z = 6.854$ via the detection of the [C II] 158 μm line. The [C II] luminosity of COS-3018 is $L_{[\rm C\,II]} = (4.7 \pm 0.5) \times 10^8\,{\rm L}_\odot$ (Smit et al. 2018). Both the spatially resolved UV and [C II] emission have been re-analysed by Carniani et al. (2018), who by using the Kennicutt & Evans (2012) UV-SFR calibration [$\log({\rm SFR}/{\rm M}_\odot\,{\rm yr}^{-1}) = \log(L_{\rm UV}/{\rm erg\,s}^{-1}) - 43.35$] derived ${\rm SFR}_{\rm UV} = 18.9 \pm 1.5\,{\rm M}_\odot\,{\rm yr}^{-1}$. The Kennicutt & Evans (2012) relation assumes Kroupa initial mass function, ≈10 Myr as mean stellar age producing the UV emission, and $Z = {\rm Z}_\odot$ for the stellar metallicity. The galaxy is instead undetected in dust continuum (Smit et al. 2018). COS-3018 is a compact galaxy: the size of the [C II]-emitting region is $r_{[\rm C\,II]} = 2.6 \pm 0.5$ kpc (Carniani et al. 2018), while the star-forming region traced by the rest-frame UV emission is considerably smaller, $r_{\rm UV} = 1.3 \pm 0.1$ kpc (Carniani et al. 2018). As both [C II] and UV emissions are marginally resolved, we can compute the [C II] surface brightness $\Sigma_{[\rm C\,II]} = L_{[\rm C\,II]}/\pi r^2_{[\rm C\,II]} = (2.2 \pm 0.7) \times 10^7\,{\rm L}_\odot\,{\rm kpc}^{-2}$, and the SFR surface density $\Sigma_{\rm SFR} = {\rm SFR}_{\rm UV}/\pi r^2_{\rm UV} = 3.6 \pm 0.5\,{\rm M}_\odot\,{\rm yr}^{-1}\,{\rm kpc}^{-2}$. This translates into $\Delta_{[\rm C\,II]} = -0.74$.

The C III] λ1909 Å emission has been detected with XSHOOTER/VLT at 4σ ($f_{\rm C\,III]} = 1.33 \pm 0.31 \times 10^{-18}\,{\rm erg\,s\,cm}^{-2}$; Laporte et al. 2017), yielding $L_{\rm C\,III]} = (1.9 \pm 0.4) \times 10^8\,{\rm L}_\odot$ and, by assuming $r_{\rm UV}$ to be a proxy of the size of the nebular line emitting region, we derive $\Sigma_{\rm C\,III]} = L_{\rm C\,III]}/\pi r^2_{\rm UV} = (3.7 \pm 0.4) \times 10^7\,{\rm L}_\odot\,{\rm kpc}^{-2}$. This is a reasonable assumption as C III] and UV continuum trace ionized gas, and the C III] 1D spectrum is extracted from the UV-emitting region. All quantities are presented in Table 1.

Table 1. Observed properties of COS-3018. Data from Carniani et al. (2018) (1), Smit et al. (2018) (2), and Laporte et al. (2017) (3).

Quantity	Value	Reference
$r_{\rm UV}$ (kpc)	1.3 ± 0.1	(1)
${\rm SFR}_{\rm UV}$ (${\rm M}_\odot\,{\rm yr}^{-1}$)	18.9 ± 1.5	(1)
$\Sigma_{\rm SFR}$ (${\rm M}_\odot\,{\rm yr}^{-1}{\rm kpc}^{-2}$)	3.6 ± 0.5	(1)
$L_{[\rm C\,II]}$ ($10^8\,{\rm L}_\odot$)	4.7 ± 0.5	(2)
$r_{[\rm C\,II]}$ (kpc)	2.6 ± 0.5	(1)
$\Sigma_{[\rm C\,II]}$ (${\rm L}_\odot\,{\rm kpc}^{-2}$)	$(2.2 \pm 0.7) \times 10^7$	This work
$L_{\rm C\,III]}$ (${\rm L}_\odot$)	$(1.9 \pm 0.4) \times 10^8$	(3)
$\Sigma_{\rm C\,III]}$ (${\rm L}_\odot\,{\rm kpc}^{-2}$)	$(3.7 \pm 0.4) \times 10^7$	This work

From the MCMC procedure, we derive the best-fitting ($\kappa_{\rm s}$, n, Z) values and confidence intervals for COS-3018. We run `emcee` with 100 random walkers exploring the parameter space for 5×10^4 chain steps. The chains have been initialized by distributing the walkers in a small region around $Z = 0.2\,{\rm Z}_\odot$, $\log(n/{\rm cm}^{-3}) = 2.5$, and $\kappa_{\rm s} = 1$. The $Z = 0.2\,{\rm Z}_\odot$ value is equal to that assumed by Bowler et al. (2014) for the stellar metallicity in their SED fitting of COS-3018. As a caveat, we note that differences between stellar and gas metallicities are likely to occur in high-z systems (Steidel et al. 2016).

We assume uniform priors for the gas density in the range $1.0 \leq \log(n/{\rm cm}^{-3}) < 3.3$, metallicity $0.05 < (Z/{\rm Z}_\odot) \leq 1.0$, and burstiness parameter $0.1 \leq \kappa_{\rm s} \leq 50$. To estimate the effective number of independent samples, we calculate the $n_{\rm burn}$ steps necessary to ensure chain independence. We adopt $n_{\rm burn} = 50\tau$, where $\tau = 147$ is the average autocorrelation time in chain steps computed with

[2]There is a (lensed) source (A383-5.1/5.2) at slightly lower redshift ($z = 6.02$; Richard et al. 2011), detected both in [C II] and C III] (Stark et al. 2015; Knudsen et al. 2016). However, given that (i) [C II] and C III] emissions have been observed in two different images, thus requiring a careful evaluation of the impact of the lens model, and (ii) the [C II] emission is only tentatively resolved, hence yielding uncertainties in the estimate of $\Sigma_{[\rm C\,II]}$, we defer a detailed study to a forthcoming paper.

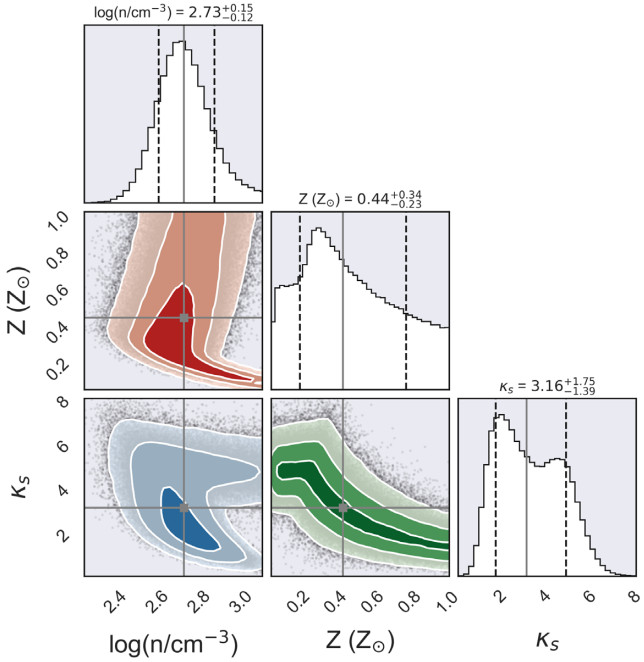

Figure 1. Corner plot showing the posterior probability distributions of $\log n$, Z, and κ_s for COS-3018 at $z = 6.854$. The contours represent 1σ, 2σ, and 3σ levels for the 2D distributions. The best-fitting parameters and the 16 and 84 per cent percentiles are plotted with grey squares and dashed lines, respectively.

the built-in implementation given in `emcee`.[3] Next, we discard the burn-in chunk and use the remaining portion to sample the posterior probability. The mean acceptance fraction is 0.504. For the best-fitting parameters and confidence levels, we use the median and the 16th and 84th percentiles of the marginal PDFs (Foreman-Mackey et al. 2013).

The result of the MCMC analysis is shown in Fig. 1. The best-fitting gas density in COS-3018 is $\log(n/\mathrm{cm}^{-3}) = 2.73^{+0.15}_{-0.12}$, which is in an excellent agreement with the mean gas density $\log(n/\mathrm{cm}^{-3}) \approx 2.5$ of dense neutral/molecular gas found by cosmological zoom-in simulations of prototypical LBGs at $z \approx 6$–7 (Pallottini et al. 2019). Such a high density value might also explain the non-detection of the C III] λ1907 Å line (Laporte et al. 2017) in this object.

The best-fitting burstiness parameter is $\kappa_s = 3.16^{+1.75}_{-1.39}$, implying that COS-3018 is a moderate starburst galaxy. Note that the presence of an ongoing starburst in COS-3018 has been tentatively suggested by previous studies (Smit et al. 2018) because of the high equivalent width of optical emission lines (EW([O III] + H β) = 1424 ± 43 Å) (Smit et al. 2015). The κ_s distribution resulting from our analysis shows a double-peak profile, with a lower peak at $\kappa_s \approx 2$ and the higher one at $\kappa_s \approx 5$. We explain this behaviour as follows. There are two possibilities to reproduce the observed [C II]/C III] ratio. The first one corresponds to a low-metallicity solution with $Z \approx 0.2\,\mathrm{Z}_\odot$, and $\kappa_s \approx 5$. In this case, the [C II] flux is higher as $N_{\mathrm{PDR}} \propto Z^{-1}$. To compensate for the [C II] increase, higher κ_s, and consequently higher U, values are required, resulting in large ionized gas column densities boosting the C III] emission (see F19). The second peak at $\kappa_s \approx 2$ corresponds to a higher metallicity ($Z \approx 0.7\,\mathrm{Z}_\odot$), which produces a thinner PDR region emitting the [C II]. In this situation, in order to fit the observed ratio a lower κ_s value is obtained. Note that the plateau at $Z \lesssim 0.2\,\mathrm{Z}_\odot$ happens because in this regime the [C II] luminosity is independent on Z as $N_{\mathrm{H\,I}} > N_0$ and hence $N_{\mathrm{PDR}} \approx N_0$ (see F19). In this region of the parameter space, Z is essentially unconstrained. Finally, our MCMC analysis constrains the gas-phase metallicity of COS-3018 in the range $Z = 0.44^{+0.34}_{-0.23}\,\mathrm{Z}_\odot$ such that, despite the large scatter due to the above considerations, it allows us to safely conclude that COS-3018 is less chemically evolved than the Milky Way but not extremely metal poor.

Note that while our method simultaneously constrains κ_s, Z, and n, in principle one can use the [C II] luminosity alone to estimate the burstiness parameter. Extrapolating the $z \approx 1$ relation $M_g = 30 L_{[\mathrm{C\,II}]}$ (mean absolute deviation of 0.2 dex; Zanella et al. 2018) to the EoR, one finds $\Sigma_g = 30 L_{[\mathrm{C\,II}]}/\pi r^2_{[\mathrm{C\,II}]} = (7.2 \pm 3.6) \times 10^8\,\mathrm{M}_\odot\,\mathrm{kpc}^{-2}$. By inverting equation (1), we get $\kappa_s = 1.43 \pm 1.0$, which is consistent within $\approx 1\sigma$ with the best-fitting κ_s found with our MCMC.

4 DISCUSSION AND CONCLUSIONS

We have presented a novel method to simultaneously determine the star formation law, gas density, and metallicity of galaxies in the EoR. This is done by exploiting the [C II] and C III] surface brightness, and the deviation from the local $\Sigma_{[\mathrm{C\,II}]}$–$\Sigma_{\mathrm{SFR}}$ relation. The method is based on an MCMC algorithm that allows us to determine the best-fitting κ_s, n, and Z of a galaxy, and their confidence levels. In particular, we analysed the case of COS-3018 an LBG at $z = 6.854$, finding that it is a moderate starburst galaxy ($\kappa_s = 3.16^{+1.75}_{-1.39}$), with a subsolar gas-phase metallicity ($Z = 0.44^{+0.34}_{-0.23}\,\mathrm{Z}_\odot$) and a mean gas density of $\log(n/\mathrm{cm}^{-3}) = 2.73^{+0.15}_{-0.12}$, in very nice agreement with predictions from state-of-the-art simulations of EoR galaxies (Pallottini et al. 2019).

The only other LBG at the end of the EoR for which the KS relation has been constrained is HZ10, for which Pavesi et al. (2019) estimated $\Sigma_g \approx 10^{10}\,\mathrm{M}_\odot\,\mathrm{kpc}^{-2}$ and $\Sigma_* \approx 10^{1.2}\,\mathrm{M}_\odot\,\mathrm{yr}^{-1}\,\mathrm{kpc}^{-2}$. They also point out that HZ10 has a very low $\kappa_s \approx 0.1$ value, compared to the other LBG in their sample (HZ6) that was undetected in CO. The HZ10/HZ6 CO luminosity ratio is >6.5, in spite of a more modest factor of 3 in their SFR ratio. They proposed that the difference in CO luminosity could be due to: (1) variation in star formation efficiency and/or (2) low-Z/dust abundance suppressing CO emission in HZ6. Our method can help clarifying this point in these and similar EoR systems. In spite of the success of the method, there are some caveats to keep in mind. The first one is that, by construction, the ISM of the galaxy is approximated with a single gas slab, with a unique density and Z. This is obviously a simplification as the [C II] and C III] emission might not be fully co-spatial. Moreover, different gas phases in the ISM show density variations throughout the galaxy.

Nevertheless, our method offers the first glimpse of global (spatially averaged) properties of EoR galaxies. As essentially no alternative constraints are currently available for EoR sources, our model can provide a first-order estimate of their key ISM properties. The obvious advantage is that it can constrain metallicity, mean gas density, and – more importantly – the SF law in large samples of sources by using only two emission lines that are detectable by ALMA, current optical/NIR telescopes, and, in the near future, *JWST*.

[3]The sampler should be run for $>10\tau$ steps before walkers fill the relevant parts of parameter space and becomes an independent set of samples from the distribution (Foreman-Mackey et al. 2013).

ACKNOWLEDGEMENTS

LV acknowledges funding from the European Union's Horizon 2020 research and innovation programme under the Marie Skłodowska-Curie agreement no. 746119. AF and SC acknowledge support from the ERC Advanced Grant INTERSTELLAR H2020/740120. AF is partially supported by the C.F. von Siemens-Forschungspreis der Alexander von Humboldt-Stiftung Research Award.

REFERENCES

Asplund M., Grevesse N., Sauval A. J., Scott P., 2009, ARA&A, 47, 481
Behrens C., Pallottini A., Ferrara A., Gallerani S., Vallini L., 2018, MNRAS, 477, 552
Bigiel F., Leroy A., Walter F., Brinks E., de Blok W. J. G., Madore B., Thornley M. D., 2008, AJ, 136, 2846
Bouwens R. J. et al., 2015, ApJ, 803, 34
Bowler R. A. A. et al., 2014, MNRAS, 440, 2810
Bowler R. A. A., Dunlop J. S., McLure R. J., McLeod D. J., 2017, MNRAS, 466, 3612
Capak P. L. et al., 2015, Nature, 522, 455
Carilli C. L., Walter F., 2013, ARA&A, 51, 105
Carniani S. et al., 2018, MNRAS, 478, 1170
Coppin K. E. K. et al., 2007, ApJ, 665, 936
Curtis-Lake E. et al., 2016, MNRAS, 457, 440
D'Odorico V. et al., 2018, ApJ, 863, L29
Daddi E. et al., 2010, ApJ, 714, L118
Dayal P., Ferrara A., 2018, Phys. Rep., 780, 1
De Looze I. et al., 2014, A&A, 568, A62
de los Reyes M., Kennicutt Robert C. J., 2019, ApJ, 872, 16
Dessauges-Zavadsky M. et al., 2015, A&A, 577, A50
Ding J. et al., 2017, ApJ, 838, L22
Feltre A., Charlot S., Gutkin J., 2016, MNRAS, 456, 3354
Ferland G. J. et al., 2017, Rev. Mex. Astron. Astrofis., 53, 385
Ferrara A. et al., 2019, MNRAS, 489, 1 (F19)
Foreman-Mackey D. et al., 2013, emcee: The MCMC Hammer, Astrophysics Source Code Library, record ascl:1303.002
Genzel R. et al., 2015, ApJ, 800, 20
Goodman J., Weare J., 2010, Commun. Appl. Math. Comput. Sci., 5, 65
Hashimoto T. et al., 2019, PASJ, 71, 71
Heiderman A., Evans N. J., II, Allen L. E., Huard T., Heyer M., 2010, ApJ, 723, 1019
Herrera-Camus R. et al., 2015, ApJ, 800, 1
Hodge J. A., Riechers D., Decarli R., Walter F., Carilli C. L., Daddi E., Dannerbauer H., 2015, ApJ, 798, L18
Hollenbach D. J., Tielens A. G. G. M., 1999, Rev. Mod. Phys., 71, 173
Hutchison T. A. et al., 2019, ApJ, 879, 70
Jaskot A. E., Ravindranath S., 2016, ApJ, 833, 136
Kawamata R., Ishigaki M., Shimasaku K., Oguri M., Ouchi M., Tanigawa S., 2018, ApJ, 855, 4
Kennicutt Robert C. J., 1998, ApJ, 498, 541
Kennicutt R. C., Evans N. J., 2012, ARA&A, 50, 531
Knudsen K. K., Richard J., Kneib J.-P., Jauzac M., Clément B., Drouart G., Egami E., Lindroos L., 2016, MNRAS, 462, L6
Kohandel M., Pallottini A., Ferrara A., Zanella A., Behrens C., Carniani S., Gallerani S., Vallini L., 2019, MNRAS, 487, 3007
Laporte N., Nakajima K., Ellis R. S., Zitrin A., Stark D. P., Mainali R., Roberts-Borsani G. W., 2017, ApJ, 851, 40
Mainali R. et al., 2018, MNRAS, 479, 1180
Maiolino R. et al., 2015, MNRAS, 452, 54
Matthee J. et al., 2019, ApJ, 881, 124
Nakajima K. et al., 2018, A&A, 612, A94
Pallottini A., Ferrara A., Gallerani S., Vallini L., Maiolino R., Salvadori S., 2017, MNRAS, 465, 2540
Pallottini A. et al., 2019, MNRAS, 487, 1689
Pavesi R., Riechers D. A., Faisst A. L., Stacey G. J., Capak P. L., 2019, ApJ, 882, 168
Richard J., Kneib J.-P., Ebeling H., Stark D. P., Egami E., Fiedler A. K., 2011, MNRAS, 414, L31
Schmidt M., 1959, ApJ, 129, 243
Schruba A. et al., 2011, AJ, 142, 37
Sharda P., Federrath C., da Cunha E., Swinbank A. M., Dye S., 2018, MNRAS, 477, 4380
Sharda P. et al., 2019, MNRAS, 487, 4305
Shibuya T., Ouchi M., Harikane Y., 2015, ApJS, 219, 15
Smit R. et al., 2015, ApJ, 801, 122
Smit R. et al., 2018, Nature, 553, 178
Stark D. P. et al., 2015, MNRAS, 450, 1846
Stark D. P. et al., 2017, MNRAS, 464, 469
Steidel C. C., Strom A. L., Pettini M., Rudie G. C., Reddy N. A., Trainor R. F., 2016, ApJ, 826, 159
Tacconi L. J. et al., 2013, ApJ, 768, 74
Tilvi V. et al., 2013, ApJ, 768, 56
Vallini L., Gallerani S., Ferrara A., Pallottini A., Yue B., 2015, ApJ, 813, 36
Vallini L., Pallottini A., Ferrara A., Gallerani S., Sobacchi E., Behrens C., 2018, MNRAS, 473, 271
Zanella A. et al., 2018, MNRAS, 481, 1976

This paper has been typeset from a TEX/LATEX file prepared by the author.